A Journal of the Gesellschaft Deutscher Chemiker

Angewandte International Edition Chemie

GDCh

www.angewandte.org

Accepted Article

Title: Hydrogen Evolution on Electrode-Supported Ptn Clusters: Ensemble of Hydride States Governs the Size Dependent Reactivity

Authors: Zisheng Zhang, Tsugunosuke Masubuchi, Philippe Sautet, Scott L. Anderson, and Anastassia N. Alexandrova

To be cited as: *Angew. Chem. Int. Ed.* **2023**, e202218210

Link to VoR: https://doi.org/10.1002/anie.202218210

WILEY VCH

10.1002/anie.202218210

WILEY-VCH

RESEARCH ARTICLE

Hydrogen Evolution on Electrode-Supported Pt_n Clusters: Ensemble of Hydride States Governs the Size Dependent Reactivity

Zisheng Zhang,[†[a]] Tsugunosuke Masubuchi,[†[b]], Philippe Sautet,[a, c, d] Scott L. Anderson*[b], Anastassia N. Alexandrova*[a, d]

Dedication: None

[a] *Z. Zhang,[†] Prof. P. Sautet, Prof. A. N. Alexandrova**
Department of Chemistry and Biochemistry
University of California, Los Angeles
607 Charles E. Young Drive, Los Angeles, CA 90095–1569, USA
E-mail: ana@chem.ucla.edu
[b] *Dr. T. Masubuchi,[†] Prof. S. L. Anderson**
Department of Chemistry
University of Utah
315 South 1400 East, Salt Lake City, UT 84112, USA
E-mail: anderson@chem.utah.edu
[d] *Prof. P. Sautet*
Department of Chemical and Biomolecular Engineering
University of California, Los Angeles
5531 Boelter Hall, Los Angeles, CA 90095–1569, USA
[d] *Prof. P. Sautet, Prof. A. N. Alexandrova**
California NanoSystem Institute
University of California, Los Angeles
570 Westwood Plaza, Los Angeles, CA 90095–1569, USA

Supporting information for this article is given via a link at the end of the document.

Abstract: We report the size-dependent activity and stability of supported $Pt_{1,4,7,8}$ for electrocatalytic hydrogen evolution reaction, and show that clusters outperform polycrystalline Pt in activity, with size-dependent stability. To understand the size effects, we use DFT calculations to study the structural fluxionality under varying potentials. We show that the clusters can reshape under H coverage and populate an ensemble of states with diverse stoichiometry, structure, and thus reactivity. Both experiment and theory suggest that electrocatalytic species are hydridic states of the clusters (~2 H/Pt). An ensemble-based kinetic model reproduces the experimental activity trend and reveals the role of metastable states. The stability trend is rationalized by chemical bonding analysis. Our joint study demonstrates the potential- and adsorbate-coverage-dependent fluxionality of subnano clusters of different sizes and offers a systematic modeling strategy to tackle the complexities.

Introduction

Developing active and low-cost electrocatalysts is the key to unlock various energy and environmental applications and sustainable chemical production. For noble metal catalysts, an important approach is to downsize the metal particles, to maximize the fraction of metal atoms in the reactant-accessible surface layer.[1] Subnano clusters, lying in between the better understood single-atom and nanoscale catalyst limits, are interesting because they often have non-monotonic size-dependence of reactivity arising from size-dependent electronic and geometric structure. Even at room temperature, subnano clusters can isomerize among various isomers,[2] requiring a statistical ensemble theoretical representation.[3,4] Moreover, the electrode potential, the interaction with the electrode support, and binding of adsorbates can further reshape the energy landscape, populating catalytic isomers with novel structures that are not accessible to bare clusters.[5] All these factors result in unique sub-nano cluster chemistry, such as breaking linear free energy relationships that constrain catalysis by bulk metals or large nanoparticles.[6,7]

Recent progress in experimental techniques enables synthesizing size-selected clusters on various conductive supports.[8] Heiz, Arenz, and coworkers[9,10] built an experimental instrument to reveal electrocatalytic processes that take place on size-selected Pt clusters and nanoparticles for the oxygen reduction reaction (ORR) and potential-induced sintering. Vajda and coworkers[11–13] reviewed size- and composition-dependent cluster catalysis and electrocatalysis, and have also reported several cluster electrochemistry studies with strong size effects.[14,15] Von Weber *et al.* revealed non-monotonic order-of-magnitude variations in the activity of Pt_n (n = 1–14) deposited on indium tin oxide (ITO) electrodes for the electrochemical oxidation of ethanol,[16] and showed that the catalytic activity correlated with the electronic structure of Pt_n probed by X-ray photoelectron spectroscopy (XPS). The same Pt_n/ITO electrodes exhibited, in contrast, monotonic effects as a function of cluster size on the branching between water and H_2O_2 products in ORR.[17] Finally,

10.1002/anie.202218210

in a recent non-electrochemical study, specific Pt clusters (most notably Pt_{10}) on titania (TiO_2) were reported to show high and stable catalytic activity toward the *photo*-induced production of H_2 compared to Pt_1/TiO_2.[18]

Herein, we present a joint experimental and theoretical study of the activity and stability of size-selected $Pt_{1,4,7,8}$ clusters deposited fluorine-doped tin oxide (FTO) electrode supports, towards the electrocatalytic hydrogen evolution reaction (HER). Mass-selected deposition in ultra-high vacuum (UHV) was used to prepare electrodes with identical Pt loadings, differing only in cluster size. These were studied by cyclic voltammetry and chronoamperometry in 0.1 M $HClO_4$ electrolyte. Because all the electrodes had identical numbers of Pt atoms, the effects of the cluster size are not complicated by coverage variations. To model the electrodes, systematic global optimizations were performed to sample the support hydroxylation, anchoring locations of clusters, cluster geometries, and adsorbate coverages and configurations, from which we established a grand canonical ensemble representation of each Pt_n/FTO electrode. By grand canonical density functional theory (GC-DFT) calculations and an ensemble-based kinetic model, we revealed the HER catalytic state to be Pt hydride clusters, with drastic structural rearrangements induced by high H coverage, and obtained a simulated size-dependent activity trend that is semi-quantitatively consistent with experiments. *Ab initio* molecular dynamics simulations and electronic structure analysis of the H-covered cluster isomer ensembles also allowed rationalizing the experimentally observed trends in size-dependent stability and support effects on activity. This study provides insights into the energetics, dynamics, and chemical bonding involved in the potential- and adsorbate coverage-induced cluster rearrangements, as well as the resulting non-monotonically size-dependent reactivity.

Results and Discussion

Cluster size-dependent HER activity

Fig. 1 shows the CVs for the 0.03 ML Pt_n/FTO (n = 1, 4, 7, 8) electrodes in the potential range between –0.137 and 0.573 V vs. RHE, plotted in terms of the measured currents. The data from the second complete CV cycle on each sample are shown as colored curves, and the data from the first CV cycles are shown as gray curves. For Pt_1/FTO and Pt_4/FTO, there were small differences between the first and second CVs, but for Pt_7/FTO and Pt_8/FTO, the two are nearly indistinguishable. In this Fig., raw currents (dashed curves) are shown to allow comparison to the background currents observed for Pt-free FTO. The FTO electrode makes negligible non-faradaic (capacitive) contributions to the CVs, but the Fig. shows that the Pt_n/FTO electrodes have additional currents that are strongly size dependent, representing the HER activity of the Pt_n/FTO catalysts. The HER activity is the smallest for the Pt_1/FTO electrode, increases substantially for Pt_4/FTO, and increases further for Pt_7/FTO and Pt_8/FTO. Because the electrodes all have the same Pt mass loading, these differences directly show the relative HER activities for the different Pt_n. The first and second CVs being nearly identical implies that the clusters were stable on this time scale, at least.

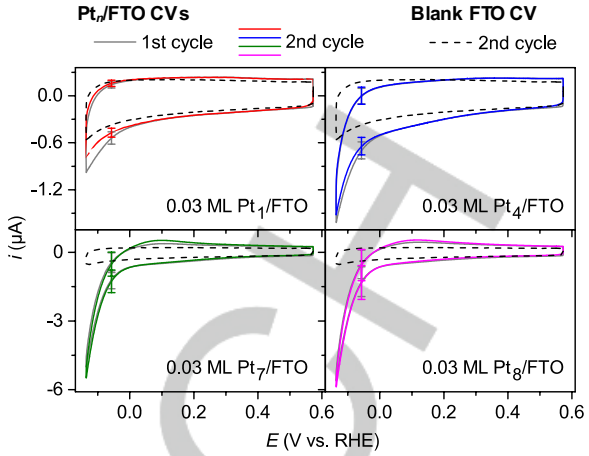

Fig. 1. CVs obtained for 0.03 ML Pt_n/FTO (n = 1, 4, 7, 8) in Ar-saturated 0.1 M $HClO_4$ at a scan rate of 0.1 V s^{-1}. For each cluster electrode, the first and second CV cycles are shown as gray and colored solid curves. The dashed curves show the second CV for blank (Pt-free) FTO recorded under the identical conditions. The error bars represent the standard deviations of repeated measurements.

To allow quantitative analysis and comparison to theory, the capacitive background currents were subtracted from the Pt_n/FTO currents to obtain the faradaic HER responses shown in Fig. 2a (left hand scale). Because we precisely know the amount of Pt present in each Pt_n/FTO (0.434 ng), the background-subtracted currents, i.e., the currents associated with the Pt clusters, are also reported in terms of mass activity, i.e., current *per* milligram Pt (right hand scale). The mass activities follow the trend of $Pt_1<Pt_4<Pt_7\approx Pt_8$.

Significant background-subtracted currents are observed at potentials positive of the HER thermodynamic threshold. These currents result from adsorption of H^+ via the one-electron Volmer step ($H^+ + e^- \rightarrow H_{ads}$), and thus track increasing numbers of H_{ads} on the electrodes as the potential decreases toward the HER threshold (vertical line, Fig. 2a). The magnitudes of these "hydrogen under-potential deposition" (H_{upd}) currents are strongly dependent on Pt_n size, roughly correlating with the HER currents observed at more negative potentials. By integrating the currents over the H_{upd} range (shaded area in Fig. 2a), the total number of

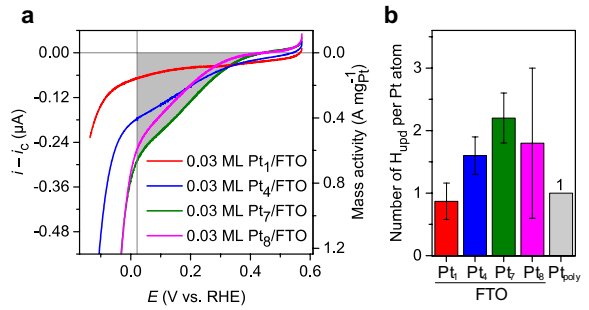

Fig. 2. (a) Negative linear sweep voltammograms for 0.03 ML Pt_n/FTO (n = 1, 4, 7, 8), obtained by subtracting the capacitive current from FTO, j_c (represented with dashed curves in Fig. 1), from the second CVs (colored solid curves in Fig. 1). The subtracted currents were integrated to calculate the total charge transferred in the H_{upd} potential region (assumed to extend to 0.023 V, where the slopes become steeper). For instance, the integration area for Pt_7/FTO is shaded gray. The electrolyte pH is assumed to ~1. (b) The size-dependent numbers of H atoms *per* Pt atom adsorbed in the H_{upd} region, calculated from the integrated H_{upd} currents from (a), co-plotted together with that for polycrystalline Pt (Pt_{poly}). The error bars represent the standard deviations of repeated measurements.

10.1002/anie.202218210

H_{ads} present at the onset of HER can be obtained. The numbers of H_{ads} over the H_{upd} potential range are shown in Fig. 2b and Table S1. Note that H_{upd} on polycrystalline Pt (Pt_{poly}) is known to result in roughly one H_{ads} per surface Pt atom,[19] and that is also the case for Pt_1/FTO. For the larger clusters, however, the H_{ads} numbers are significantly higher, at ~2 H_{ads}/Pt atom.

This H_{upd} analysis assumes that no other reactions contributed to the background-subtracted currents in the H_{upd} potential range. We considered the possible contribution from the oxygen reduction reaction (ORR) due to O_2 contamination of the electrolyte, despite extensive Ar purging. We measured ORR currents for Pt_n/FTO samples in $HClO_4$ with added O_2, and the result (Fig. S4) is that the ORR onset potential is well above the onset potential for the H_{upd} currents in Fig. 2a, leading us to conclude that the contribution from this background process can be neglected.

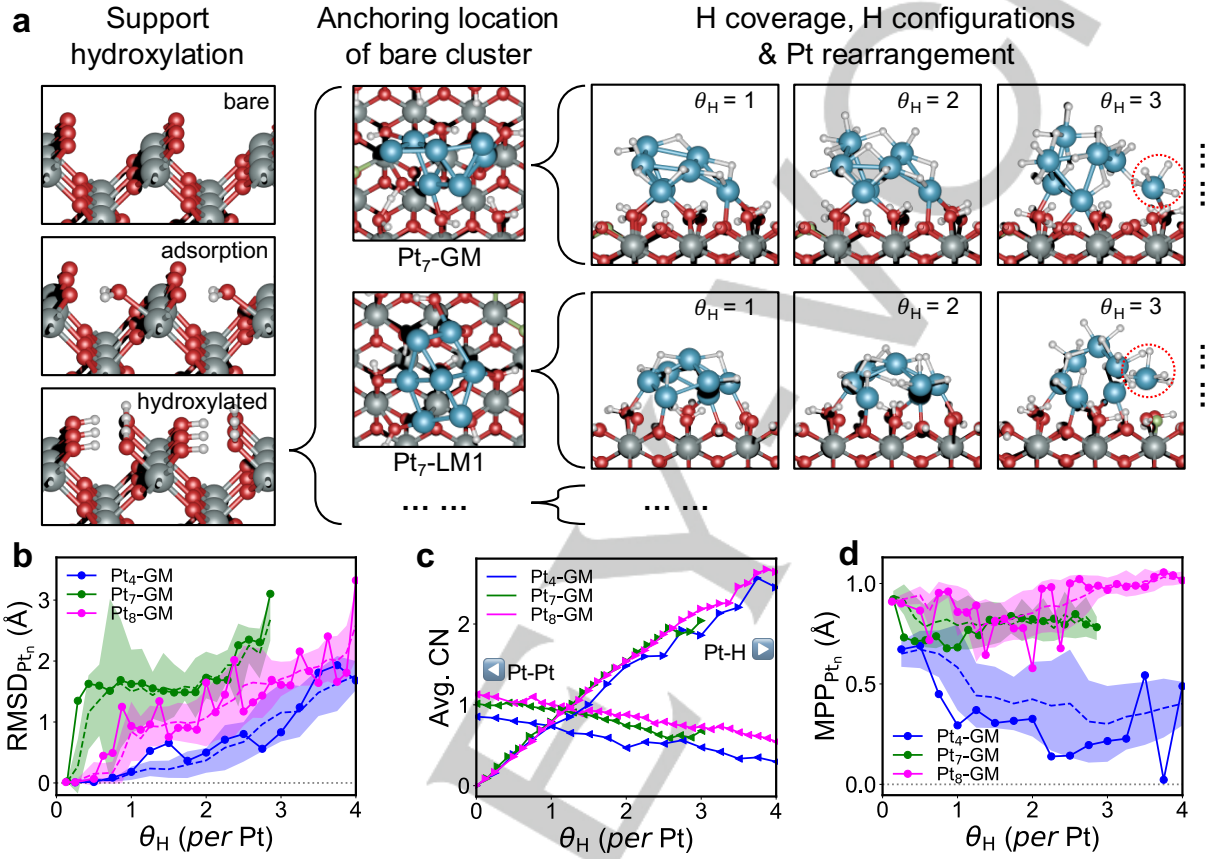

Fig. 3. (a) Representation of the Ptn/FTO system. The hydroxylation of support, different anchoring locations of bare clusters, and the structure of H-covered clusters are addressed by global optimization structure searches. Representative structures of Pt_7 are shown in insets, with notable motifs highlighted by red dotted circles. (b) RMSD of the core geometries of $Pt_{4,7,8}$-GM versus H coverage, referenced against the H-free bare cluster geometries. (c) Averaged coordination numbers of Pt-Pt and Pt-H pairs in the $Pt_{4,7,8}$-GM versus H coverage. (d) The molecular planarity parameter (MPP) of cluster core of $Pt_{4,7,8}$-GM versus H coverage. The solid curves with round markers mark the most stable structure of each coverage. The dashed curves and shaded areas represent the mean and distribution (within one standard deviation) of all sampled structures of each coverage.

The Structure of Pt_n/FTO under HER conditions

To understand the size-dependent HER activity of FTO-supported subnano Pt clusters, we need a realistic model of the Pt_n/FTO system under relevant conditions. The structure of the support is built based on a doped stoichiometric tin oxide (100) termination, as described in the methods section and in the SI. Since the reaction takes place in aqueous media, we expect the FTO surface to be heavily covered by water. Global optimization of water on tin oxide adsorbed at 0 to 1 ML coverage is performed, and GC-DFT calculations are performed on the low-energy minima of each coverage to obtain potential-dependent electronic free energies. The water configuration is found to depend on the water coverage (Pourbaix diagram in Fig. S7a): At low coverage (1/3 ML), water coordinates to exposed Sn sites via O and stays intact. At high coverage (1 ML), adsorbed water dissociates, transferring one H to a neighboring bridge O to form two hydroxyls. Such hydration/hydroxylation phenomena have been reported for various metal oxide surfaces.[20,21] In the relevant range of the applied potential, and at room temperature and ambient pressure, the FTO surface is expected to be completely hydroxylated (Supplementary Note 1).

Global optimizations are performed for Pt clusters of size 1 to 8 atoms on hydroxylated FTO (Fig. S7b, Supplementary Note 2) to sample the relevant low-energy cluster configurations. A rather wide distribution of structures is obtained, with diverse anchoring locations on the FTO support. By Boltzmann statistics, multiple cluster configurations are accessible at room temperature and without applied potential. For example, the global minimum (GM) and the 1st local minimum (LM1) of bare Pt_7 have populations of 79.18% and 12.34%, respectively. The structures and populations of accessible isomers of $Pt_{1,4,7,8}$/FTO at room temperature are plotted in Fig. S7c. Since a typical barrier

10.1002/anie.202218210

for cluster migration over the surface is calculated to be 0.82 eV (Fig. S8), we do not expect the clusters to be mobile on the FTO support at room temperature. However, the barriers for cluster isomerization are found to be significantly lower (0.2~0.5 eV, dependent on adsorbate coverage, see Fig. S9); hence, we assume that at each binding location on the support, the cluster can access all its isomers and obeys Boltzmann statistics. Exhaustive sampling of all possible barriers to migration and isomerization is prohibitively expensive, but our earlier studies showed that assuming Boltzmann statistics is a reasonable approximation, judging by agreement of theory with experiment.[22–26] Local fluxionality (as opposed to global) also has been noticed,[27] and is expected at lower electrocatalysis temperatures.

At an electrochemical interface, the electrode potential and the chemical potential of the adsorbates are constant, hence the net charge and the adsorbate coverage could vary as the cluster isomerizes and as the reaction progresses. This constitutes a grand canonical ensemble (of electrons and adsorbates) containing cluster states with diverse structures and stoichiometries. The geometric and electronic properties depend nontrivially on the adsorbate coverage and configuration.[28] Here we use the grand canonical genetic algorithm (GCGA) to efficiently sample the structural and compositional space of H-covered Pt_n (n=1,4,7,8) on hydroxylated FTO (details in Fig. S10-11 and Supplementary Note 4). Again, we assume that there is no cluster migration and the H coverage and cluster configurations are sampled only on the accessible anchoring locations (Fig. S7).

The geometries of Pt_7 on hydroxylated FTO under different H coverages are shown in Fig. 3a. The core structure of the cluster reshapes significantly as the coverage increases, as is evidenced by the root-mean-square deviation (RMSD) of Pt atoms as a function of H coverage (Fig. 3b). The average coordination number (CN) of Pt-H increases at higher H coverage. Meanwhile, the Pt-Pt CN gradually decreases with increasing H coverage (Fig. 3c). The change in shape of the cluster core is quantified by the molecular planarity parameter (MPP)[29] in Fig. 3d. Bare clusters of all sizes start with globular structures, and then flatten as the H_{ads} coverage increases to ~1 H per Pt (H atoms cap the periphery of the cluster to make it spread). Then, at higher coverages, the planarity is broken, and the cluster becomes globular again, but as a hydride. The isomerization of the cluster core is facilitated by H adsorbates: The barrier of Pt_7 reshaping into a flatter core configuration is lowered from 0.49 eV to 0.23 eV after adsorption of merely two H (Fig. S9).[30]

Ensemble-level understanding of the HER activity trends

Since multiple isomers of cluster configurations with different H coverages are predicted to coexist under HER conditions, multiple active sites and reaction pathways may be important. Assuming that the cluster core can rearrange within the timescale of the HER elementary steps, we can construct a reaction network consisting of all possible HER pathways connecting any two structures with neighboring H coverages (e.g., Pt_nH_x and Pt_nH_{x+1}).[5] Diverse reaction energetics emerge from ensemble of metastable structures, forming a gaussian-like distribution of H-adsorption free energy, ΔG_H. Taking the GM of Pt_8 (Fig. 4a) as an example, the distribution of ΔG_H broadens with increasing H coverage due to increased diversity of sites, and the center of the distribution shifts from over-binding to ~0 eV, suggesting overall improved HER energetics. Since subnano clusters generally have stronger binding with adsorbates compared to the bulk terminations, the HER energetics for Pt clusters at high H coverage become closer to that for Pt(111) and to the theoretical optimum of $|\Delta G_H| = 0$.

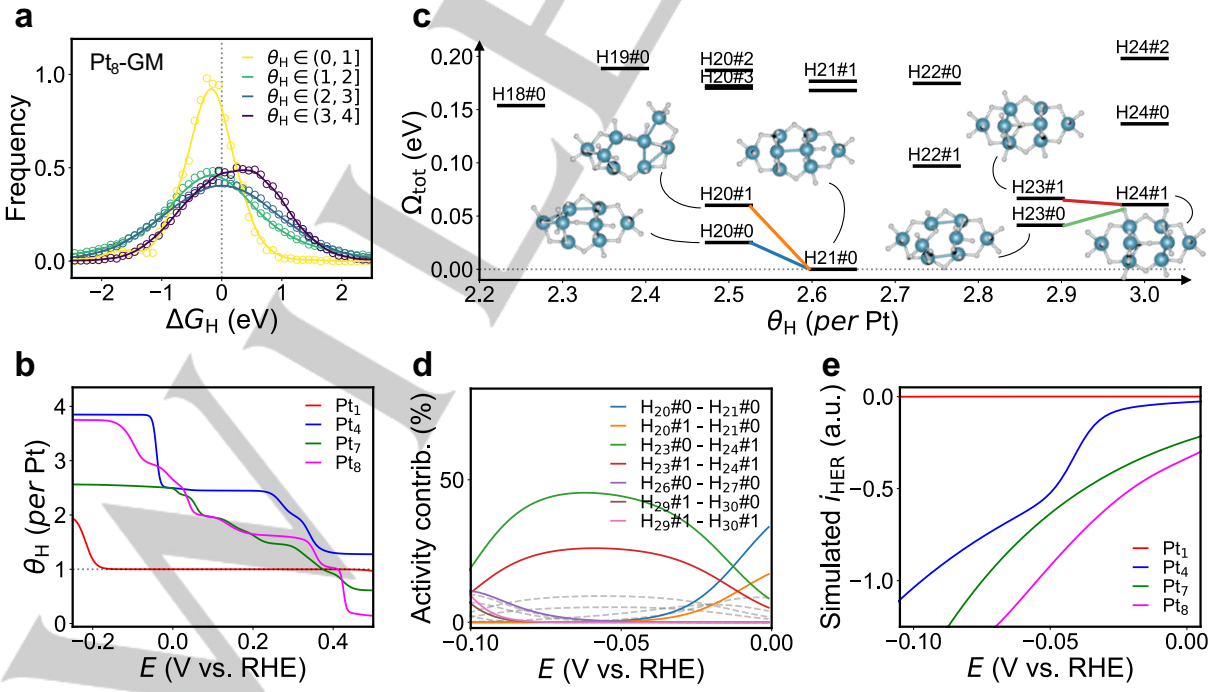

Fig. 4. (a) Distribution of H adsorption free energy for all possible (H_n, H_{n+1}) reaction pairs on Pt_8-GM in different ranges of H coverage (*per* Pt). (b) Potential-dependent H coverages of $Pt_{1,4,7,8}$/FTO, including all anchoring locations and H-covered configurations. (c) Schematics of the accessible metastable states of Pt_8-GM under H coverage at 0 V_{RHE}, with notable reaction pairs marked by colored dotted lines and structures shown as insets. (d) HER activity contribution from

10.1002/anie.202218210

stable and metastable states in the HER potential regime for Pt_8-GM. (e) Simulated HER activity of $Pt_{1,4,7,8}$/FTO, including contribution from all cluster anchoring locations and H coverages.

However, the structures with optimal HER energetics may not be accessible. To find the Pt_nH_x/FTO structures that are accessible at relevant electrode potentials, a grand canonical representation can be constructed by performing GC-DFT calculations on the low-energy structures of each H coverage. The result is a potential-dependent grand canonical free energy Ω (of adsorbate and electron) which can be used to calculate the population of each structure according to Boltzmann statistics. In Fig. 4b, the averaged H coverage of the cluster configurations are calculated as a function of the electrode potential. Near the HER onset, $Pt_{4,7,8}$ already have a high H coverage of ~2.5 H/Pt, which is in excellent agreement with experimental results in Fig. 2b. Such high H coverage is a result of structural flexibility of subnano clusters enabling H insertion into a hydride-like form.

After obtaining the pair-wise HER energetics and the relative population of each Pt_nH_x/FTO structure, we calculate the HER activity for each cluster size using an ensemble-based activity model[5] which assumes: (i) Any two states with neighboring H coverage can make a HER cycle of $\mathrm{Pt}_n\mathrm{H}_x \rightarrow \mathrm{Pt}_n\mathrm{H}_{x+1} \rightarrow \mathrm{Pt}_n\mathrm{H}_x + \mathrm{H}_2$ (adding H^+ at each step); (ii) All elementary steps of HER obey an Arrhenius rate expression with the same preexponential factor; (iii) The reaction barrier correlates linearly with the reaction free energy (i.e., assuming a Bell-Evans-Polyani relationship[31]) for all elementary steps of HER; (iv) The concentration of active species is determined solely by Boltzmann statistics according to grand canonical free energy.

Fig. 4c is a schematic of accessible H-covered Pt_8 states at 0 V_{SHE}, with H_x#m representing the m-th local minimum of the Pt_8H_x composition from the neutral charge DFT calculations during the GCGA sampling. Note that the ordering can change as the electrode potential sweeps, and thus #m serve merely as a label. It can be seen, the actual catalyst consists of hydride clusters, with two contributing HER pathways connecting states of H_{20} and H_{21}. Moreover, metastable structures such as H_{20}#0 and H_{20}#1 contribute a non-negligible fraction of the total activity, up to ~20% (Fig. 4d). As the electrode potential sweeps negative, there is a crossover of the major activity contributors, with the $H_{20,21}$ states depleted and $H_{23,24}$ states populated. The significant contribution from metastable structures, and the changing H coverages on the most important activity contributors are observed also in other cluster configurations (Fig. S13). This potential-dependent shift in H coverage and in the most populated and active species is also in line with the non-linear Tafel curve in Fig. S14. At low overpotential, below 50 mV, the Tafel slope is rather large (> 200 mV/dec), suggesting little HER activity as the cluster is not yet hydrogenated into an activated hydride form. As overpotential increases, the $Pt_{4,7,8}$ are gradually hydrogenated and activated, with the Tafel slope continuously decreasing until converging at c.a. 125 mV/dec, 95 mv/dec, and 88 mv/dec, respectively. The change in Tafel slope suggests a shift of the rate limiting step from Volmer ($H^+ + e^- \rightarrow H_{ads}$) to Heyrovsky ($H_{ads} + H^+ + e^- \rightarrow H_2$) , as the H coverage on the clusters builds up.[33] The Tafel slope of Pt_1, however, does not undergo significant changes or converge to a specific value, likely because it cannot form any stable state with higher H coverage beyond ~1 H/Pt_1. Thus, unlike bulk metal or larger bulk-like nanoparticles, the fluxional subnano metal clusters (but not Pt_1) can adsorb large amounts of H and undergo dramatic structural change in the process, and therefore interpreting Tafel slopes by comparing to results for bulk-like electrodes is unreliable.

By summing up the contributions from all pairs of structures for all cluster binding locations, we can calculate the total HER activity for each cluster size (normalized by amount of Pt) as a function of applied potential (Fig. 4e). An activity trend of Pt_8>Pt_7>Pt_4>Pt_1 is obtained, consistent with the experimental trend in Fig. 1 and 2.

The size dependence of activity arises from the different distributions of HER energetics among the accessible structures for each Pt_n. A broader distribution of ΔG_H (Fig. S15), indicating a a higher diversity of states and a continuous spectrum of pair-wise energetics, leads to a higher HER activity. The energetic diversity is also associated with structural diversity (Fig. 3b), sharing roughly the same trend of Pt_1<Pt_4<$Pt_7 \approx Pt_8$. Note that the accessibility of a Pt_nH_x state also depends on its relative stability with respect to states of neighboring H coverages (Pt_nH_{x-1} and Pt_nH_{x+1}) in terms of grand canonical free energy, resulting in a complex relationship to which there is no analytical solution.

Stability of the Pt_n/FTO and the origin of size dependence

Fig. 5a and b show chronoamperometry (CA) results at potentials of -0.057 V and 0.063 V vs. RHE, respectively. At -0.057 V, which is negative of the thermodynamic HER threshold, all four systems undergo activity decay to some extent, with Pt_7/FTO and Pt_8/FTO exhibited substantial decay of their initially high HER currents. This suggests that the supported clusters, especially Pt_7/FTO and Pt_8/FTO, might have undergone some deactivation process under HER conditions.

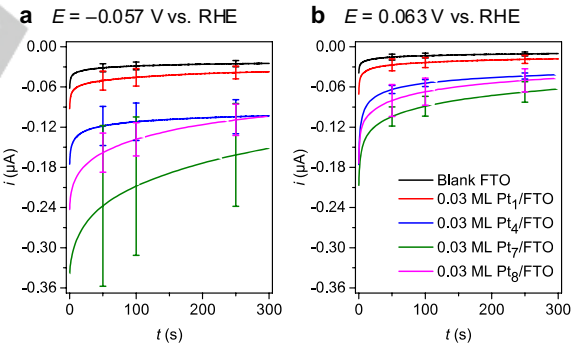

Fig. 5. Chronoamperometry of 0.03 ML Pt_n/FTO (n = 1, 4, 7, 8) and blank FTO electrodes in Ar-saturated 0.1 M $HClO_4$ at applied potentials of (a) –0.057 and (b) 0.063 V vs. RHE. The error bars represent the standard deviations of repeated measurements.

The potential 0.063 V (Fig. 5b) is 40 mV positive of the HER threshold under the experimental conditions (0.023 V vs. RHE), however, because the H_2 partial pressure in our experiments is negligible, there may be significant HER activity at this potential. In addition, the non-electrochemical H-removal processes noted above would free up sites for continuing slow H adsorption, adding to the currents. At the more negative potential, the Pt_7 and Pt_8 currents were observed to decay more rapidly than those for Pt_4 and Pt_1. In the CA measurements (Fig. 5a), the size dependence of the initial HER currents is Pt_1<Pt_4<Pt_8<Pt_7, but because the Pt_7 and Pt_8 currents decayed over time more rapidly than Pt_4, by the end of the 300 second experiments, the activity

10.1002/anie.202218210

ordering was Pt_1<Pt_4≈Pt_8<Pt_7. The stability could be quantified by fitting the background-subtracted current in Fig. 5a to the Cottrell equation under the assumption that the surface concentration of active species decays exponentially with respect to time, or by the percentage decay of current during the 300 s measurement, both yielding a stability trend of Pt_1<Pt_7<Pt_8<Pt_4 (Supplementary Note S6).

Note that the initial activity order in Fig. 5 is also different from that seen in the CVs, shown in Figs. 1 and 2. We believe that this is a result of the CA being measured after the CV scans which caused changes to the electrodes. To test this possibility, Fig. S16 shows another set of CA experiments run under the same conditions as in Fig. 5, also with CVs run first, however, the potential range of those CVs was narrowed. In the CVs preceding the experiments in Fig. 5, the upper potential limit was 0.573 vs. RHE, whereas the CVs run prior to the experiments shown in Fig. S16 had an upper potential limit of just 0.273 V vs. RHE. As can be seen in that Fig., the narrowed potential window appears to have reduced the changes to the electrodes or catalysts, such that the initial activity order was the same as in the CVs, i.e., Pt_1<Pt_4<Pt_7<Pt_8. The activity decay behavior was quite similar, i.e., Pt_7 and Pt_8 decaying much faster than Pt_4. Thus, it appears that in addition to activity decaying under HER conditions, significant decay also occurs if the potential is scanned too far positive. We did not test the effects of cycling to higher upper potential limits because, as shown above, the cluster H coverage, geometries, and Pt-Pt bond strengths vary with H coverage. Thus, cycling to high potentials changes the cluster structure and bonding, and for high enough potentials, can lead to Pt oxidation. The concern is these changes likely promote Pt dissolution or sintering.

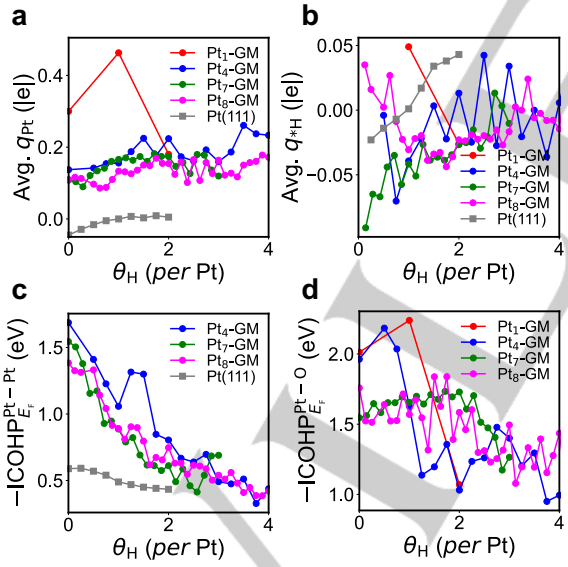

Fig. 6. (a) Averaged DFT-calculated Bader charge of surface Pt atoms and (b) H adsorbates in the most stable structures of H-covered $Pt_{1,4,7,8}$/FTO and Pt(111) versus H coverage (*per* Pt atom in the cluster or in the top surface). Integrated Crystal Orbital Hamilton Population up to Fermi level ($ICOHP_{Ef}$) of (c) Pt-Pt within the surface layer or the cluster core and (d) Pt-O between cluster and support of the most stable structures of H-covered $Pt_{1,4,7,8}$/FTO and/or Pt(111), versus H coverage.

The distinct size dependent activity and stability has an electronic structure origin. In Fig. 6a, within the relevant range of H coverage (up to ca. 1H/Pt for Pt_1 and Pt(111), up to ~2H/Pt for $Pt_{4,7,8}$), the averaged Bader charge on Pt follows the order of Pt_1>Pt_4>Pt_7>Pt_8>Pt(111)≈0, i.e. single supported Pt atoms are cationic, while the surface of metallic bulk Pt is nearly charge neutral, with the Pt_n clusters lying between. As a result, when covered with ~2H/Pt, smaller clusters are more cationic, which is associated with higher lying *d* states and a tendency to bind H more strongly.[34] Since Pt(111) has near-optimal energetics for HER, subnano Pt clusters, and expecially Pt_1, would in general tend to over-bind H as their size decreases.

The charge state of H_{ads} also changes as the H coverage increases (Fig. 6b). In general, H_{ads} becomes more acidic and weakly bound at higher H coverage. There are some anomalies where H_{ads} gets more hydridic in the low coverage regime (0—1), due to structural rearrangements of the cluster core. Notably, at the high H coverage limit of c.a. 4 *per* Pt, some accessible states feature H spillover from the H-saturated cluster to the FTO support (Fig. S17), which is the most likely process accounting for the non-electrochemical loss of H_{ads} proposed above to explain the weakness of H_{ads} desorption signals at slow scan rates (Fig. S5b and S5c). We expect that H spillover to the FTO should be more significant for highly hydrogenated clusters than for larger supported Pt nanoparticles, because of both the higher H coverages, and the proximity of H binding sites to FTO. Indeed, efficient spillover of adsorbed species to oxide supports has been observed for subnano Pt-based catalysts.[34–38] The fate of the spilled-over H atoms is not known, but possibilities include protonation of surface oxo/hydroxyl, incorporation into the FTO lattice, or recombinative desorption as H_2.

Higher H coverage also leads to weaker intra-cluster Pt-Pt bonds (unlike in Pt(111)), as is indicated by the Crystal Orbital Hamilton Population (COHP) analysis (Fig. 6c), and broadening and shift to longer distance of the Pt-Pt radial distribution function (RDF), reminiscent of melting (Fig. S12c). The Pt-O bonds binding the cluster to the support also weaken and lengthen with increasing H coverage (Fig. 6d and Fig. S12d). However, the coverage effect on Pt-O bonds is much smaller than for the Pt-Pt bonds, with only a slight shift of the Pt-O RDF peak. The weakening of the Pt-Pt bonding allows partial detachment of peripheral Pt atoms from the cluster (Fig. 3a). The detached Pt_1 would suffer more from the weakening of Pt-O upon H adsorption than larger clusters, since there are no Pt-Pt to stabilize it. Hence, we expect that Pt_1 is more prone to dissolution, which explains the worst stability of Pt_1 in Fig. 5. Although complete detachment of the hydrogenated peripheral Pt is not observed in the 10-ps AIMD simulation, we expect that hydrogenated peripheral Pt atoms may break off from the cluster cores during the electrocatalysis. Because HER activity decreases with decreasing cluster size, this process would lead to an overall activity decrease, even though the number of Pt atoms present on the catalyst is unchanged. This fluxionality-driven deactivation is similar to the case of Pt_n/TiO_2,[39] but here the final state would be isolated and inactive Pt_1 structures formed by detachment of peripheral Pt atoms, rather than the more usual case of ripening into larger particles (which would boost the HER activity).

The Pt-Pt and Pt-O bond strengths do not follow a monotonic trend with cluster size: Pt-Pt bond strength is Pt_4>Pt_8≈Pt_7, consistent with HER stability trend observed (Fig. 5) but reverse from the activity trend (Pt_4<Pt_7<Pt_8, Fig. 1). Although increasing cluster size generally leads to weaker intra-cluster bonding, higher structural diversity, better HER activity, and worse HER stability (*vide supra*), Pt_7 and Pt_8 do not follow the

trend. The underlying reasons are complex and associated with the "ensemble size"[4] being rather unpredictable for intermediate size clusters.

Comparisons with Pt_n on different supports and with Pt_{poly}

Here we compare the HER mass activities for Pt_n/FTO with the activity of Pt_{poly}, and with that for Pt_n supported on indium tin oxide (ITO),[40] measured under identical conditions. Fig. 7 compares the mass activities for Pt_n/FTO and Pt_n/ITO (n = 1, 4, 7, 8) at a potential of –0.027 V vs. RHE, corresponding to an overpotential η = 0.05 V, based on currents measured in the CVs in Fig. 2a, and analogous CVs reported for Pt_n/ITO.[40] The size dependences are generally similar, but all four Pt_n/FTO samples were significantly more active than the corresponding Pt_n/ITO at η = 0.05 V. For Pt_1, the activity on FTO, although small, was more than double that on ITO, and for the larger, more active clusters, the FTO support is more active by ~20%.

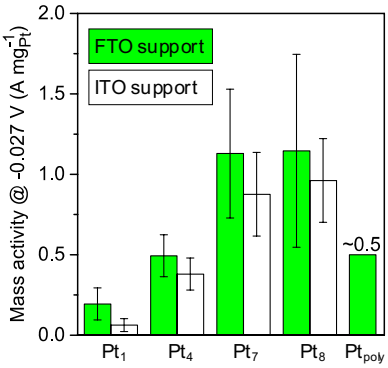

Fig. 7. Comparison of mass activities toward the HER for 0.03 ML Pt_n/FTO (*n* = 1, 4, 7, 8), 0.03 ML Pt_n/ITO (*n* = 1, 4, 7, 8), and Pt_{poly} obtained under identical conditions at –0.027 V vs. RHE, corresponding to an overpotential η = 0.05 V.

To compare to a well-defined HER standard, Fig. 7 also includes the activity of polycrystalline Pt (Pt_{poly}), measured in the same cell under identical conditions. We calculated a "top-layer mass activity" for Pt_{poly} by dividing the current measured for Pt_{poly} by the mass of just the electrolyte-exposed top monolayer of the Pt_{poly} electrode (see Fig. S5a), assuming one H atom adsorbing *per* exposed Pt atom in the H_{upd} potential range.[19] The result is a value of ~0.5 A/mg_{Pt}, and because the normalization mass includes only the top layer, this value is an upper limit on the mass activity for bulk Pt or bulk-like Pt-containing electrodes.

For Pt_1 on both FTO and ITO, the mass activity is well below the Pt_{poly} limit, for Pt_4 the values are comparable to the Pt_{poly} limit, and for both Pt_7 and Pt_8, the mass activities are roughly double the limiting value for Pt_{poly}. In essence, isolated Pt atoms on FTO or ITO have HER activities substantially lower than the activity *per* surface layer atom for Pt_{poly}. The activity *per* Pt atom for Pt_4/FTO is similar to the activity *per* surface Pt atom in Pt_{poly}, while that for Pt_4/ITO is ~20% lower. For Pt_7/FTO and Pt_8/FTO, the activities *per* Pt atom are more twice that for the surface atoms in Pt_{poly}.

However, the larger Pt_n/FTO lose activity relatively rapidly, compared with Pt_4/FTO and all the Pt_n/ITO, such that the activity for $Pt_{7,8}$/FTO drops below the activities for $Pt_{7,8}$/ITO after a few minutes. The lower stability of the larger Pt_n on FTO may be due to high surface hydroxylation, compared to ITO.[41] Thus, Pt clusters might anchor more strongly (via oxo sites) on ITO, compared to anchoring via hydroxyls on FTO. The difference in cluster/support interaction strength also may partly explain the higher activity of Pt_n/FTO compared to Pt_n/ITO for the same cluster sizes, because Pt_n/ITO would be more cationic and therefore have overly-strong Pt-H binding, compared to FTO. The high activity observed for Pt_1/FTO, compared to Pt_1/ITO may reflect the weaker binding of Pt_1 on hydroxyl-saturated FTO, compared to the less hydroxylated ITO surface, allowing a small degree of sintering to form small Pt_n/FTO, with significantly higher activity than isolated atoms. In summary, the higher initial activity but lower stability for Pt_n/FTO, compared to ITO, can be rationalized in terms of the binding properties of the supports, as-hydroxylated under aqueous conditions.

Conclusion

In summary, we studied the electrocatalytic hydrogen evolution reaction on size-selected subnano Pt clusters supported on fluorine-doped tin oxide *via* a combination of experiment and theory. The catalytic species are revealed to be coexisting cluster structures with high H coverage (ca. 2 H *per* Pt), featuring hydride-like motifs. An ensemble-based kinetic model is used to simulate the net HER rate for different cluster sizes, with excellent agreement with the trend of experimental activity (Pt_1<Pt_4<Pt_7≈Pt_8). The stability trend of Pt_4>Pt_8>Pt_7>Pt_1 is rationalized by the size- and coverage-dependent charge state of Pt atoms, and the intra-cluster and cluster-support bond strengths. In particular, the non-monotonic size dependences of bond strengths, structural diversity, and distribution of isomer energetics jointly determines the activity and stability trends. The support effects on activity and stability are attributed to different cluster-support interaction strengths at different extents of hydroxylation. This work highlights the importance of potential- and adsorbate-coverage-dependent structural rearrangements of subnano clusters in determining the size-dependent activities, and the necessity of including catalyst structures of diverse compositions, configurations, and energetics in order to correctly model fluxional systems under reaction conditions.

The focus of this work is fundamental, but from a practical perspective, the results indicate that true single-atom Pt/oxide electrode catalysts would have poor activity for HER, but that sub-nano clusters can be quite active, exceeding the activity of the surface atoms in bulk-like Pt. The finding of size- and adsorbate coverage-dependent fluxionality, and its effects on activity and stability, are likely relevant in any catalysis by sub-nano clusters. Similarly, the finding that the clusters convert to hydrides at potentials relevant to HER should hold for somewhat larger clusters, and even for the first few top layers of bulk crystalline surfaces.[30,42] We do plan additional experiments on larger clusters, different metals, and different supports, and measurements of the Hupd currents will address the H:metal ratio. Obviously, the effects of these properties on specific systems, with different metals, supports, and reactions, are likely to be different.

Acknowledgements

This work is supported by grant DE-SC0020125 from the U.S. Department of Energy, Office of Science, Basic Energy Science Program. The computations in this work were performed on:

Hoffman2 the UCLA-shared cluster; Cori and Perlmutter of the National Energy Research Scientific Computing Center (NERSC), a U.S. Department of Energy Office of Science User Facility operated under Contract DE-AC02-05CH11231; Theta of the Innovative and Novel Computational Impact on Theory and Experiment (INCITE) program at the Argonne Leadership Computing Facility, a U.S. Department of Energy Office of Science User Facility operated under Contract DE-AC02-06CH11357. SLA acknowledges support for the Henry Eyring Presidential Endowed Chair funds. We thank Prof. Henry S. White for helpful discussions regarding this work, and Ashley Cass and Simran Kumari for discussing experimental and computational details, respectively. We thank Gunther Andersson and Abdulaziz Almutairi (Flinders Univ. Physics) for providing the XPS survey data for FTO.

Conflict of Interest

The authors declare no conflict of interest.

Keywords: Ab initio calculations • Cluster catalysis • Electrochemistry • Fluxionality • Hydrogen evolution reaction

[1] L. Liu, A. Corma, *Chem. Rev.* **2018**, *118*, 4981–5079.

[2] T. Imaoka, T. Toyonaga, M. Morita, N. Haruta, K. Yamamoto, *Chem. Commun.* **2019**, *55*, 4753–4756.

[3] Z. Zhang, B. Zandkarimi, A. N. Alexandrova, *Acc. Chem. Res.* **2020**, *53*, 447–458.

[4] R. H. Lavroff, H. W. T. Morgan, Z. Zhang, P. Poths, A. N. Alexandrova, *Chem. Sci.* **2022**, *13*, 8003–8016.

[5] Z. Zhang, Z.-H. Cui, E. Jimenez-Izal, P. Sautet, A. N. Alexandrova, *ACS Catal.* **2020**, *10*, 13867–13877.

[6] Z. Zhang, B. Zandkarimi, J. Munarriz, C. E. Dickerson, A. N. Alexandrova, *ChemCatChem* **2022**, *14*, e202200345.

[7] B. Zandkarimi, A. N. Alexandrova, *J. Phys. Chem. Lett.* **2019**, *10*, 460–467.

[8] A. von Weber, S. L. Anderson, *Acc. Chem. Res.* **2016**, *49*, 2632–2639.

[9] S. Kunz, K. Hartl, M. Nesselberger, F. F. Schweinberger, G. Kwon, M. Hanzlik, K. J. J. Mayrhofer, U. Heiz, M. Arenz, *Phys. Chem. Chem. Phys.* **2010**, *12*, 10288–10291.

[10] M. Nesselberger, S. Ashton, J. C. Meier, I. Katsounaros, K. J. J. Mayrhofer, M. Arenz, *J. Am. Chem. Soc.* **2011**, *133*, 17428–17433.

[11] S. Vajda, M. G. White, *ACS Catal.* **2015**, *5*, 7152–7176.

[12] A. Halder, L. A. Curtiss, A. Fortunelli, S. Vajda, *J. Chem. Phys.* **2018**, *148*, 110901.

[13] G. Kwon, G. A. Ferguson, C. J. Heard, E. C. Tyo, C. Yin, J. DeBartolo, S. Seifert, R. E. Winans, A. J. Kropf, J. Greeley, R. L. Johnston, L. A. Curtiss, M. J. Pellin, S. Vajda, *ACS Nano* **2013**, *7*, 5808–5817.

[14] C. Yin, F. Zheng, S. Lee, J. Guo, W.-C. Wang, G. Kwon, V. Vajda, H.-H. Wang, B. Lee, J. DeBartolo, *J. Phys. Chem. A* **2014**, *118*, 8477–8484.

[15] J. Lu, L. Cheng, K. C. Lau, E. Tyo, X. Luo, J. Wen, D. Miller, R. S. Assary, H. H. Wang, P. Redfern, H. Wu, J. B. Park, Y. K. Sun, S. Vajda, K. Amine, L. A. Curtiss, *Nat. Commun.* **2014**, *5*, 4895.

[16] A. von Weber, E. T. Baxter, S. Proch, M. D. Kane, M. Rosenfelder, H. S. White, S. L. Anderson, *Phys. Chem. Chem. Phys.* **2015**, *17*, 17601–17610.

[17] A. von Weber, E. T. Baxter, H. S. White, S. L. Anderson, *J. Phys. Chem. C* **2015**, *119*, 11160–11170.

[18] M. Eder, C. Courtois, P. Petzoldt, S. Mackewicz, M. Tschurl, U. Heiz, *ACS Catal.* **2022**, *12*, 9579–9588.

[19] B. E. Conway, B. V. Tilak, *Electrochim. Acta* **2002**, *47*, 3571–3594.

[20] R. Mu, Z. Zhao, Z. Dohnálek, J. Gong, *Chem. Soc. Rev.* **2017**, *46*, 1785–1806.

[21] G.-J. Xia, Y.-G. Wang, *Chinese J. Chem. Phys.* **2022**, *35*, 629–638.

[22] E. T. Baxter, M.-A. Ha, A. C. Cass, A. N. Alexandrova, S. L. Anderson, *ACS Catal.* **2017**, *7*, 3322–3335.

[23] E. T. Baxter, M.-A. Ha, A. C. Cass, H. Zhai, A. N. Alexandrova, S. L. Anderson, *J. Phys. Chem. C* **2018**, *122*, 1631–1644.

[24] T. J. Gorey, B. Zandkarimi, G. Li, E. T. Baxter, A. N. Alexandrova, S. L. Anderson, *J. Phys. Chem. C* **2019**, *123*, 16194–16209.

[25] M. A. Ha, E. T. Baxter, A. C. Cass, S. L. Anderson, A. N. Alexandrova, *J. Am. Chem. Soc.* **2017**, *139*, 11568–11575.

[26] B. Zandkarimi, T. J. Gorey, G. Li, J. Munarriz, S. L. Anderson, A. N. Alexandrova, *Chem. Mater.* **2020**, *32*, 8595–8605.

[27] H. Zhai, A. N. Alexandrova, *J. Phys. Chem. Lett.* **2018**, *9*, 1696–1702.

[28] G. Sun, P. Sautet, *J. Am. Chem. Soc.* **2018**, *140*, 2812–2820.

[29] T. Lu, *J. Mol. Model.* **2021**, *27*, 263.

[30] Z. Zhang, Z. Wei, P. Sautet, A. N. Alexandrova, *J. Am. Chem. Soc.* **2022**, *144*, 19284–19293.

[31] J. K. Nørskov, T. Bligaard, A. Logadottir, J. R. Kitchin, J. G. Chen, S. Pandelov, U. Stimming, *J. Electrochem. Soc.* **2005**, *152*, J23–J26.

[32] T. Shinagawa, A. T. Garcia-Esparza, K. Takanabe, *Sci. Rep.* **2015**, *5*, 13801.

[33] Q. Hu, K. Gao, X. Wang, H. Zheng, J. Cao, L. Mi, Q. Huo, H. Yang, J. Liu, C. He, *Nat. Commun.* **2022**, *13*, 3958.

[34] R. T. Yang, Y. Wang, *J. Am. Chem. Soc.* **2009**, *131*, 4224–4226.

[35] S. Bonanni, K. Aït-Mansour, W. Harbich, H. Brune, *J. Am. Chem. Soc.* **2012**, *134*, 3445–3450.

[36] H. Kim, J. Park, Y. S. Lee, *J. Comput. Chem.* **2013**, *34*, 2233–2241.

[37] Z.-W. Wei, H.-J. Wang, C. Zhang, K. Xu, X.-L. Lu, T.-B. Lu, *Angew. Chemie Int. Ed.* **2021**, *60*, 16622–16627.

[38] J. Dai, Y. Zhu, Y. Chen, X. Wen, M. Long, X. Wu, Z. Hu, D. Guan, X. Wang, C. Zhou, *Nat. Commun.* **2022**, *13*, 1189.

[39] B. Zandkarimi, P. Poths, A. N. Alexandrova, *Angew. Chemie Int. Ed.* **2021**, *60*, 11973–11982.

[40] S. Kumari, T. Masubuchi, A. N. Alexandrova, H. S. White, S. L. Anderson, P. Sautet, *J. Am. Chem. Soc.* **2022**, *in press*.

[41] S. Kumari, P. Sautet, *J. Mater. Chem. A* **2021**, *9*, 15724–15733.

[42] S. Hanselman, F. Calle-Vallejo, M. T. M. Koper, *J. Chem. Phys.* **2023**, *158*, 14703.

10.1002/anie.202218210

WILEY-VCH

RESEARCH ARTICLE

Entry for the Table of Contents

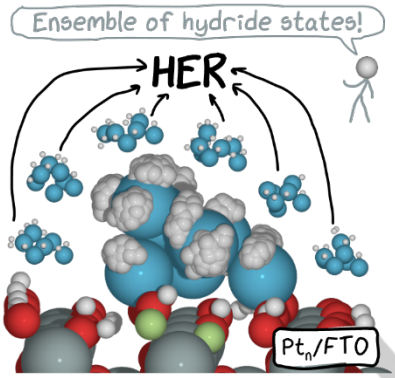

Hydrogen evolution on size-selected subnano Pt clusters supported on fluorinated tin oxide (FTO) originates from hydride-like species (ca. 2 H/Pt), which form at a reductive electrode potential and are distinct from single atoms and bulk Pt. The size dependence of activity and stability were understood based on a grand canonical ensemble representation of the catalyst states and chemical bonding analysis.

Institute and/or researcher Twitter usernames:
@uclachem
@UUtah
@zisheng_zhang_